Collision Cascade and Sputtering Process in a Polymer

A. Delcorte* and P. Bertrand

PCPM, Universite Catholique de Louvain, 1 Croix du Sud, B1348, Louvain-la-Neuve, Belgium

B. J. Garrison

Department of Chemistry, The Pennsylvania State University, 152 Davey Lab, University Park, Pennsylvania 16802

Received: March 22, 2001; In Final Form: June 13, 2001

The particle induced fragmentation and sputtering of a ~7.5 kilodalton organic sample is modeled using molecular dynamics (MD) simulations. The model system consists of a polystyrene coil containing 61 styrene repeat units adsorbed on Ag(111). It is bombarded by 500 eV Ar projectiles. To obtain a realistic picture of the dynamics for an organic material, we used the new adaptative AIREBO potential developed by Stuart, Tutein, and Harrison, which includes long-range van der Waals forces in the reactive potential created by Brenner (REBO) for hydrocarbon systems. Significant differences between the results obtained with and without the long-ranged interaction are identified. The development of the collision cascade in the organic medium is analyzed in detail using collision trees and movies of the results from the simulation. In addition to fast atomic collision processes, we show the existence of long-lived vibrational excitations and demonstrate their importance for the emission of kilodalton chain segments. Recombined and rearranged fragments are emitted, but their contribution to the mass spectrum is insignificant beyond 40 Da. Delayed emission via vibration-induced bond scission is also observed. Finally, we compare the MD results with new ToF−SIMS measurements performed in the context of this study.

1. Introduction

Organic surfaces, encompassing synthetic polymers, additives, molecular overlayers, biological molecules and tissues, are involved in a large number of technologically and medically important applications. The design and control of these systems require analysis techniques that are sensitive to the chemistry of the outermost surface layer and, if possible, are quantitative. In the past two decades, static secondary ion mass spectrometry (SSIMS), has been successfully applied to solve a variety of problems related to such surfaces, as witnessed by the success of the major conference in the field.[1] Future improvement of the method, however, requires a better understanding of the physics of organic sputtering.[2]

Using molecular dynamics (MD) simulations, a good foundation of knowledge about the emission processes has been built for many systems, including organic overlayers on inorganic substrates.[3−9] Submonolayers of limited size molecules on heavy metal substrates, even though they constitute rather specific systems, set the stage for examining organic crystals, large molecular adsorbates, or thick polymer layers.[10] A key difference with these systems is the two distinct strengths of the interaction at play, that is, strong intramolecular chemical bonds versus weak intermolecular van der Waals forces. In this new context, using the Brenner potential functions (REBO[11]) for the C−C and C−H interactions is a significant approximation because this potential does not include long-range interactions. Recently, Stuart, Tutein, and Harrison developed the adaptative intermolecular REBO potential (AIREBO), including both the reactivity of the REBO potential and the long-range van der Waals interactions.[12] This sophisticated potential has already been used to model the sputtering of solid benzene samples.[13] Another implementation of the long-range forces in the frame of the REBO potential has been developed by Beardmore and Smith. This potential has been applied to model the fullerene-induced ejection of molecular species from graphite.[14,15]

In this paper, we take avantage of the new AIREBO potential to address various issues related to the sputtering of bulk organic materials. These are, for instance, the development of a collision cascade in a coiled polymeric chain, the possible energy transfer into the vibrational modes of the molecule after a stage of high energy collisions, the expansion of the excited molecule toward the vacuum,[16] the direct or delayed fragmentation processes, the possible chemical reactions in the excited volume. In practice, we model the bombardment of a polystyrene (PS) sample adsorbed on silver by 500 eV Ar atoms. The size of the PS sample, comprising 61 styrene repeat units, has been chosen so that collision cascades can develop in its bulk, with a reduced influence of the underlying silver substrate. On the other hand, this size is sufficiently limited to be computationally tractable. The MD simulation results are compared to new experimental data and simulations conducted in the binary collision approximation.

2. Methods

2.1. Molecular Dynamics Simulation. The Ar bombardment of a *sec*-butyl terminated polystyrene oligomer (Figure 1) adsorbed on a Ag(111) surface is modeled using molecular dynamics (MD) computer simulations. The MD scheme has been described in extensive detail elsewhere.[8,17−21] It consists of integrating Hamilton's equations of motion to determine the

* Corresponding author. Phone: 32-10-473582; fax: 32-10-473452; e-mail: delcorte@pcpm.ucl.ac.be.

10.1021/jp011099e CCC: $20.00
Published on Web 09/11/2001

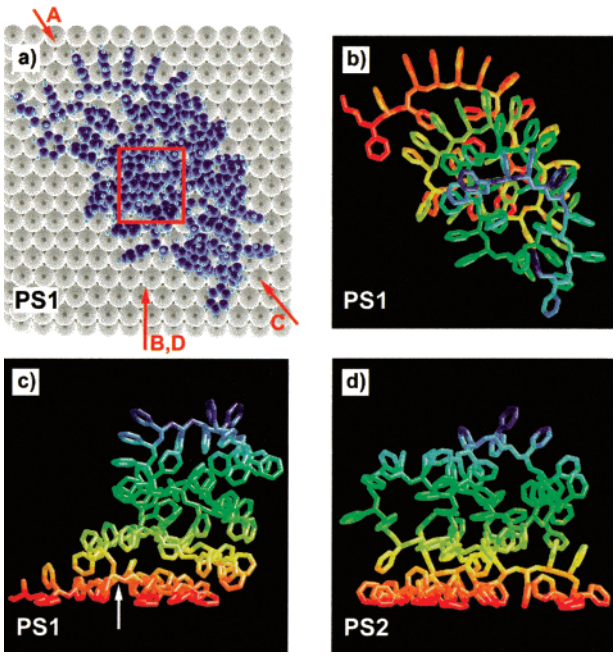

Figure 1. Surface configuration of the samples. Figure 1a shows a top view of the first sample (PS1). Silver atoms are represented by large gray spheres, carbon and hydrogen atoms by blue spheres. The bombarded area is indicated by a rectangle. The labels indicate the position of the viewer in the corresponding trajectory movies. Figure 1b and 1c show top and side views of the carbon backbone of the first sample (PS1). The situation of the side view is shown by arrow B in Figure 1a. The color range, from red to blue, indicates the height of the atoms in the molecule. The white arrow in Figure 1c indicates the bond that is broken in trajectory B (see text for details). Figure 1d shows a side view of the carbon backbone of the second sample (PS2).

position and velocity of each particle as a function of time. The energy and forces in the system are described by many-body interaction potentials. Experimentally observable properties are calculated from the final positions, velocities, and masses of all the ejected species. Mechanistic information is obtained by monitoring the time evolution of relevant collisional events.

The blend of empirical pairwise and many-body potential energy functions used to represent the forces among the various atoms has been described in previous papers,[4,7] except for the adaptative intermolecular potential, AIREBO, developed by Stuart and co-workers.[12] This potential is based on the reactive empirical bond-order (REBO) potential developed by Brenner for hydrocarbon molecules.[22,23] To overcome the limitation of the REBO potential to short-range interactions, the AIREBO potential introduces nonbonding interactions through an adaptative treatment, which conserves the reactivity of the REBO potential. In the AIREBO potential, the strength of the intermolecular forces depends on the local chemical environment of the atoms. For instance, the repulsive wall that constitutes a barrier for reaction between two methane molecules is lowered or even absent for the corresponding methyl radicals, which allows them to react. The AIREBO potential has been used in our recent MD studies of the sputtering of solid benzene.[13]

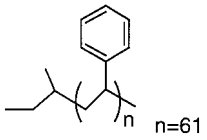

In the model, two samples of polystyrene oligomers containing 61 repeat units (PS1, PS2) have been synthesized with different coil arrangements in order to check the influence of configuration on the sputtering process. The two chain ends of the PS oligomers are a *sec*-butyl group and a H atom, respectively (see formula). The silver substrate is approximated by a finite microcrystallite containing seven layers of 208 Ag atoms for both systems. The polystyrene oligomer coil is placed on the Ag{111} surface, and the entire system is quenched to a minimum energy configuration prior to Ar atom impact. The binding energy of a PS sample is obtained by subtracting the sum of the total energy of the relaxed silver crystal and that of the PS sample (in vacuo) from the total energy of the relaxed crystal with adsorbed oligomer. With our parameters, the binding energy of one PS oligomer to the silver substrate is ~5.7 eV. Top and side views of the first sample (PS1) after relaxation are shown in Figure 1a−c. Figure 1d shows a side view of the second system (PS2). The size of each PS molecule is approximately $30 \times 30 \times 25$ Å^3. The two samples shown in Figure 1c and 1d differ only by their organization and shape. The difference in total potential energy and binding energy is insignificant. The density of the PS sample is obtained by counting the number of carbon and hydrogen atoms in a cube of 1000 Å^3. The cube is then moved across the molecule to sample different regions of its bulk. The average density obtained from 10 local density measurements is 1.04 ± 0.1 g/cm^3. In comparison, the literature reports a density of 1.05 g/cm^3 for bulk polystyrene.[24] A series of trajectories has also been calculated using PS1 and the REBO potential. For this trajectory set, the relaxed PS1 sample shown in Figure 1a−c has been quenched again within the REBO potential, i.e., suppressing long-range forces, to remove the stress induced by the potential switch. During the relaxation step, the organic sample became more compact, reaching a final density of 1.42 ± 0.2 g/cm^3.

For the bombardment itself, primary Ar atoms are directed along the surface normal. A representative set of Ar aiming points or trajectories directed within the impact area (rectangle in Figure 1) were calculated. The aiming points are regularly distributed in the impact area. The impact area is centered on the polystyrene oligomer, since our study focuses on the collision cascade and sputtering processes occurring within organic solids. More than 100 trajectories were calculated with each PS molecule in the AIREBO potential, i.e., a total of ~300 trajectories were computed. For comparison purpose, about 1000 trajectories were also calculated with the first sample (PS1) using the REBO potential. The cutoff distance of the REBO potential is three times shorter than that of the AIREBO potential. This makes the evaluation of the forces within the hydrocarbon molecule approximately 3^3 times faster with the REBO potential. Therefore, the CPU time per trajectory using the REBO potential is almost 1 order of magnitude shorter than it is using the AIREBO potential, which explains the larger number of computed trajectories.

Each trajectory is initiated using a fresh undamaged sample. Open boundary conditions are used for the system.[20] At the end of each trajectory, atoms that have a velocity vector directed away from the surface and are at a height of 8 Å above the top of the molecule are considered as sputtered atoms. In all the considered systems, the mass of hydrogen was taken to be that of tritium (3 amu) to increase the computational efficiency by increasing the time step in the numerical integration.[4] With large organic samples such as our PS oligomers, a reliable criterion for terminating trajectories is difficult to establish because vibrational motion of the entire sample may lead to the emission of large fragments with a very low kinetic energy per constituent

atom and for extremely long ejection times in comparison with smaller adsorbed molecules such as benzene.[4] On the other hand, considering that a 3 ps trajectory calculated with the AIREBO potential generally takes 24 h on a IBM-SP node, it would be unreasonable to let all trajectories run for longer time limit. Therefore, we decided to run all trajectories for a minimum duration of 2.5 ps and to monitor the number of atoms above the 8 Å boundary as a function of time. Those trajectories for which the number of ejected atoms did not saturate after the first 2.5 ps were restarted with a longer time. This stepwise procedure allows us to run trajectories over a time range encompassing the end of the ejection process, yet not compute for lengthy times when no ejection is occurring.

2.2. Secondary Ion Mass Spectrometry (SIMS). Samples of *sec*-butyl terminated, deuterated PS oligomers ($M_n = 5300$ Da) are dissolved in toluene with a concentration of 3×10^{-3} M. The samples are prepared as thin films cast on 0.25 cm^2 silver foils (Goodfellow; 99.95+ % purity), by depositing a droplet of the solution on the supports. Prior to deposition, the substrates are etched in 30% highest purity grade sulfuric acid (Vel) for 3 min, then rinsed in water of high-performance liquid chromatography (HPLC) grade from a milli-Q system (Millipore) and p.a. grade 2-propanol (Vel).

The secondary ion mass analyses and the KED measurements are performed in a PHI-EVANS time-of-flight SIMS (TRIFT 1) using a 15 keV Ga^+ beam.[25] The details of the experimental setup are described elsewhere. In this particular series of experiments, the secondary ions are post-accelerated by a 7.5 kV voltage in front of the detector to improve the measured intensities. ToF−SIMS spectra in the mass range $0 < m/z < 10000$ are obtained from 1200 s acquisitions on a 130×130 μm^2 sample area, which corresponds to a fluence of 1.1×10^{12} ions/cm^2, ensuring static bombardment conditions.

3. Results and Discussion

The scope of this article is the elucidation of the collision cascade, fragmentation and sputtering mechanisms induced by fast atoms in organic materials. The following discussion starts with the description of a typical trajectory. Then, we show the influence of the long-range forces and the effect of the molecule configuration on the molecular dynamics. The main section of this article is devoted to the explanation of the different mechanisms inducing PS fragmentation and sputtering. The substrate effect is also investigated. Finally, the simulation results are compared to recent experimental findings.

3.1. Example of a Trajectory. It is convenient to introduce the detailed analysis of the results with the visual description of a typical trajectory observed in the simulation (trajectory A, Figure 2). The chosen trajectory illustrates a category of events in which characteristic *fingerprint* fragments of PS are sputtered. The initial state of the adsorbed molecule and the position of the impinging Ar atom before starting the simulation are shown in Figure 2a. For the sake of clarity, the direction of the viewer used in Figure 2 is indicated by the arrow labeled A in Figure 1a. By 200 fs, the projectile has penetrated deeply into the molecule and all of its energy has been transferred to the organic medium via a succession of collisions. As a consequence of the first few collisions at the top of the molecule, several fragments are quickly ejected, including C and H atoms as well as CH and C_2H_2 molecules. Larger fragments are already detached from the rest of the molecule, but they are still in the field of the van der Waals forces. By 800 fs, two characteristic fragments of polystyrene, C_6H_5 and C_9H_7, have been generated. The phenyl is travelling in the vacuum while the C_9H_7 is still

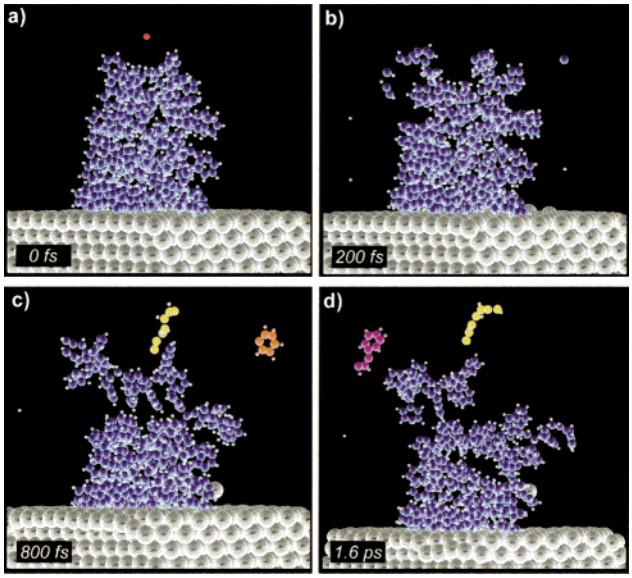

Figure 2. Time evolution of a characteristic trajectory (A). (a) 0 fs; (b) 200 fs; (c) 800 fs; (d) 1600 fs. The incident Ar atom is represented by a red sphere. The C_6H_5, C_7H_6 and C_9H_7 fragments are orange, yellow, and purple, respectively.

in the potential well of the neighboring hydrocarbon chain segments. A linear C_7H_6 is also emitted from the top of the PS molecule. Because of the internal energy excess, this fragment will decompose into C_2H_2 and C_5H_4 at approximately 2 ps. After 1.6 ps, C_9H_7 is also free and the rest of the PS molecule continues to move and vibrate under the action of the energy accumulated in its bonds. A large chain segment, detached from the main part, is hovering on top of the molecule. It will eject after ~5.5 ps.

This example helps us to identify some general features of the fast ion−organic solid interaction. First, the 500 eV Ar atom is able to dissipate all of its kinetic energy in a 25 Å thick sample, in agreement with range calculations based on Monte Carlo codes using the binary collision approximation, such as TRIM. Second, the collisions induced by the projectile in the sample lead to the ejection of single atoms and polyatomic fragments, including characteristic fragments observed in experimental mass spectra. After a first batch of collision-induced emission, the large energy excess accumulated in the sample causes a slow expansion of the chain segments. Therefore, the dynamics can span on a time scale of several tens of picoseconds. Before studying the detailed sputtering mechanisms, the following sections address the influence of the long-range force term of the hydrocarbon interaction potential and the effect of the sample arrangement on the measured quantities.

3.2. Effect of the Long-Range Forces. To test the effect of the potential nature on the sputtering process, we performed two series of simulations, one with the REBO potential limited to short range interactions and the other with the newly implemented AIREBO potential including van der Waals forces.

The mass spectra obtained with the AIREBO and the REBO potentials are shown in Figure 3a and 3b,c, respectively. For comparison, the numbers reported in Figure 3 are normalized yields per 100 trajectories for both potentials. First, it must be mentioned that the statistics collected using the AIREBO potential are too limited to proceed with a detailed quantitative comparison of the sputtering yields. In particular, it is almost impossible to make comparisons for very large fragments (>1 kDa) due to their low yield. Therefore, the high mass region of the spectrum is omitted for the AIREBO potential. This

TABLE 1: Influence of the Potentials and Initial Conditions on the Yields of Secondary Species[a]

number of traj.	total mass	total number	yields H	C	C_2H_2	C_3H_3	C_6H_5
REBO							
PS1							
1068	117.3 (a)	5.0 (a)	2.1 (a)	0.49 (a)	0.67 (a)	0.04 (a)	0.12 (a)
AIREBO							
PS1							
164	55.3 (b)	3.6 (b)	2.2 (b)	0.38 (b)	0.27 (b)	0.02 (b)	0.02 (b)
100	58.1	3.8	2.2	0.41	0.26	0.02	0.02
50	52.9	3.2	1.9	0.28	0.26	0.0	0.0
Diff. %[b]	−53	−28	+2	−23	−60	−56	−79
PS2							
134	87.2 (c)	4.3 (c)	2.3 (c)	0.31 (c)	0.38 (c)	0.04 (c)	0.08 (c)
100	90.2	4.4	2.3	0.32	0.40	0.06	0.09
50	83.0	4.3	2.4	0.32	0.36	0.08	0.06
PS1+PS2	69.6	3.9	2.2	0.35	0.32	0.03	0.05
Diff. %[c]	+58	+17	+4	−17	+41	+145	+237

[a] The second and third columns indicate the average mass and number of fragments sputtered per incident particle, respectively. [b] Derived by (b−a)/a × 100. [c] Derived by (c−b)/b × 100.

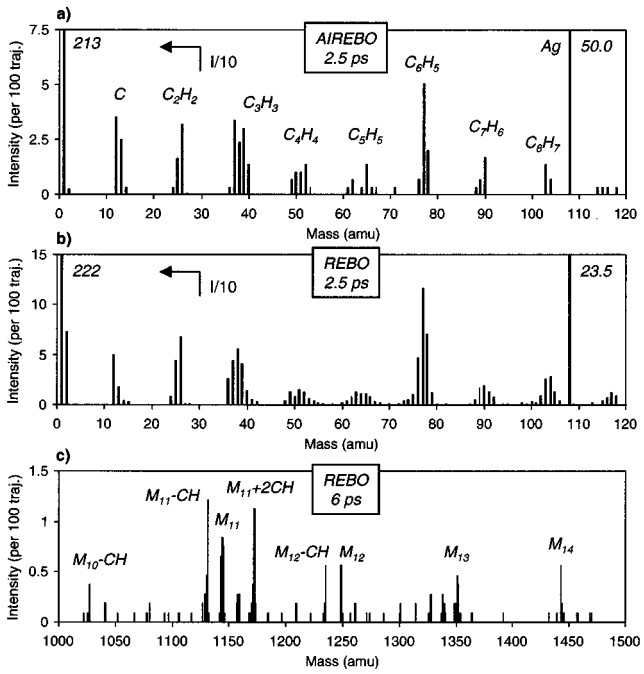

Figure 3. Calculated mass spectrum of a *sec*-butyl terminated PS 61-mer adsorbed on Ag{111} under 500 eV Ar atom bombardment (normalized yields per 100 trajectories): (a) low-mass range of the spectrum obtained after 2.5 ps using the AIREBO potential; (b) low-mass range of the spectrum obtained after 2.5 ps using the Brenner (REBO) potential; (c) high-mass range of the spectrum obtained after 6 ps using the REBO potential. Although the mass of hydrogen is 3 Da (tritium) in the simulation, it is considered as equal to 1 for comparison with experimental spectra of regular polystyrene.

limitation is only due to the large amount of CPU time required per trajectory calculated with the AIREBO potential, preventing larger numbers of trajectories to be run. Even for the low mass region shown in Figure 3a and 3b, some of the yield numbers quoted in the following paragraphs for this potential must be considered as indicative of *trends* rather than precise values. Nevertheless, beside the absolute yield issue, the *nature* and even the *relative yields* of fragments detected in both cases are quite similar, as witnessed by the overall shape of the spectra presented in Figure 3a and 3b. In both cases, the low mass fragments ($m < 30$ Da) dominate strongly, hydrocarbon series are observed up to at least 120 Da, and the dominant fragment in the range 30 Da $< m <$ 120 Da is the phenyl radical, C_6H_5.

The information concerning the yields of fragments is gathered in Table 1. The values reported in Table 1 (and Figure 3a,b) correspond to a truncation of all the trajectories at 2.5 ps. This truncation in time is necessary because the two sets of simulations have not been conducted over identical time ranges. To assess the accuracy of the AIREBO values, the convergence of the yields as a function of the number of trajectories has been tested in each case. Partial and complete results, i.e., the yields for 50, 100, and for the total number of trajectories are reported in Table 1 for the two configurations (PS1 and PS2). In this section, only the yields calculated for the first configuration (PS1) will be discussed. For the AIREBO/PS1 set, the yield values are almost stable after 100 trajectories (within a 10% variation range).

As indicated by the reasonable convergence of the yields described above, the smaller statistics with the AIREBO potential is not the major factor explaining the yield difference between the two potentials. For small fragments such as H, C, and C_2H_2, which exhibit high emission yields, the statistics are certainly sufficient for a quantitative comparison to be performed. Except for hydrogen, the sputtering yield is generally higher with the REBO potential. The difference is particularly significant for C_2H_2, whose intensity is reduced by 60% using the AIREBO potential. An important reduction (79%) is also observed for C_6H_5, though the statistics are more questionable. This trend is reflected by the total mass and total number of fragments ejected per primary particle (columns 1 and 2 in Table 1). Indeed, switching from the REBO potential to the AIREBO potential reduces the total number of fragments by 28% and the total mass by 53%, i.e., the change in number corresponds to a much larger change in mass. This observation confirms that the yield loss affects mostly high mass fragments. Moreover, our results also show that the dynamics of emission of small fragments is indeed affected by the choice of the potential, even though such fragments mainly result from high-energy collisional processes, as will be shown in section 3.4.

The difference between the two potential functions might be due either to the different structural properties of the molecule as relaxed in the REBO potential or to the increased intermolecular attractive forces themselves. On one hand, the PS1 molecule relaxed in the REBO potential (density $= 1.42 \pm 0.2$ g/cm^3) is significantly denser than that relaxed in the AIREBO potential (density $= 1.04 \pm 0.1$ g/cm^3). Because the molecule is more compact using the REBO potential, the energy deposition in the surface region might be affected, as well as the

ejection probability. On the other hand, the sum of the binding energies in the relaxed molecule is 2 % larger with the AIREBO than the REBO potential. This difference might seem negligible in terms of total potential energy, but we believe it is significant considering the sputtering process of polyatomic fragments. Indeed, the emission of fragments generally requires one or two single covalent bond-breaking events, for which the binding energy increase is actually 2% using the AIREBO potential. But, in addition to the covalent bond(s), the fragment formed in the AIREBO potential has to overcome several additional van der Waals interactions, the number of which increases with the fragment size. In these conditions, the energy required to liberate the fragment can be much larger than that needed in the REBO potential. This explanation also accounts for the observed mass effect through the proportional number of van der Waals interactions that must be overcome in order to eject the fragment. In that sense, the intermolecular forces act like a supplementary glue between neighboring chain segments in the organic solid.

3.3. Effect of the Initial Conditions. In this section, we explore the influence of the PS sample configuration on the nature and yield of sputtered species. The modification of the molecular area scanned by the primary particles for a given sample configuration should also be relevant, but the information provided would be redundant. Indeed, with our system, a change of the impact area also corresponds to scanning a region of the sample that has a different molecular arrangement. Therefore, a pronounced sensitivity to one of these parameters should imply a significant sensitivity to the other one as well.

Table 1 compares the yields of fragments measured for the two PS arrangements (Figure 1c and 1d). The overall yield values for the two systems (PS1+PS2) in the AIREBO potential are indicated for information. The convergence of the yields has been also tested for the second configuration, PS2. Again, most of the yields converge quickly, despite the small number of trajectories calculated. The yields obtained for the first 50 trajectories are indeed very close to the final values. Therefore, we believe that the differences observed between PS1 and PS2 are significant in most cases and that they relate to the different arrangements of the two samples with respect to the target area.

Hydrogen atoms exhibit similar yields, irrespective of the molecular arrangement. In the case of C atoms, a definitive conclusion cannot be drawn because the convergence is not very good for PS1. In addition to these two atomic species, all the specific yields of fragments as well as the total number of fragments and the total mass per primary particle are significantly different for the two molecular configurations. For instance, the ejected mass is 58% higher with the second system. These numbers show that the emission of fragments is largely dependent on the molecular configuration sampled by the primary particle. A practical consequence is that the SIMS relative intensities should be different for samples made of identical molecules adsorbed with different orientations on different substrates.[26]

Another indication of the influence of the molecule shape on the surface is given by the high mass range of the spectrum of PS1 obtained using the REBO potential (Figure 3c). Beyond 0.5 kDa, there is only one series of peaks, in the range 1−1.5 kDa, with a significant intensity. The mass analysis shows that these peaks correspond mostly to the formulas M_x and $M_x \pm CH$ with $11 \leq x \leq 14$ and M being the styrene repeat unit. A closer look at the PS1 sample arrangement on the surface (Figure 1b and 1c) indicates that the precursor of these fragments is the top segment of the oligomer, containing the chain end. This segment forms a half ring lying on top of the sample (blue-green). The other end of the segment is located in the bombarded region. Following the chosen aiming point, the primary particle breaks C−C bonds in this chain segment to form fragments with 11 to 14 styrene repeat units. In contrast, large fragments with less than 11 or more than 14 repeat units are almost absent of the spectrum, mainly because the C−C bond that must be broken to release them is not directly located in the target area. Our analysis of the high mass fragments thus shows that both the particular chain arrangement and the target area play a major role concerning the nature of the observed fragments.

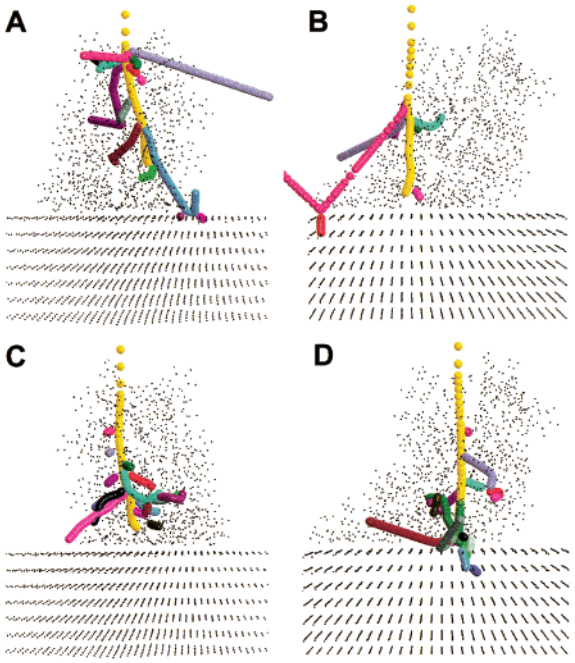

Figure 4. Collision trees of the first 100 fs of the interaction for four characteristic trajectories. The successive positions of the recoil atoms are indicated by colored spheres, provided that they are set in motion with more than 10 eV of energy. They are turned off when their energy drops below 5 eV.

3.4. Mechanisms. According to their characteristic time and energy, the processes occurring in the bombarded PS sample belong to two categories, an early atomic-like collision cascade phase and a late molecular motion phase. The existence of both types of processes has been suggested in the first place by the description of trajectory A. The first category covers what is usually referred to as the *collision cascade* itself in the literature and the ejection of fragments directly induced by fast moving atoms. The *molecular* processes take place at longer times, when the primary particle energy is distributed almost equally among a large number of atoms in the molecule, i.e., after cooling of the atomic cascade. After the analysis of these categories of mechanisms, the influence of the silver substrate on the dynamics is considered.

3.4.1. Atomic Collision Cascade. The first part of the fast atom−organic target interaction corresponds to the development of the atomic collision cascade in the solid. In relation with organic materials, atomic collision cascade and collision induced ejection have been observed for overlayers of various molecules on metal surfaces.[4−8] In contrast to these samples in which the majority of the collision cascade takes place in the substrate, in our system the collision cascade develops directly in the organic medium. Fingerprints of characteristic collision cascades are illustrated in Figure 4, using "collision trees".[9,27] In this representation, the atoms at rest are represented by black dots

and the atoms that receive 10 eV or more kinetic energy via a collision are shown as colored spheres. The colored spheres are turned off when the kinetic energy of the atoms drops below 5 eV. The collision trees summarize the successive positions of the moving atoms over the first 100 fs of the interaction. The overall aspect of the trees is not strongly dependent on the considered interaction time beyond 100 fs. Therefore, 100 fs can be considered as a characteristic time for the development of atomic cascades in the case of 500 eV Ar bombardment of polystyrene.

The collision trees illustrated in the four vignettes of Figure 4 exhibit common as well as distinctive features. The first vignette corresponds to trajectory A, described in section 3.1 and Figure 2. For 500 eV Ar bombardment, Figure 4 shows that the cascades are mostly composed of atoms hit directly by the primary Ar atom (yellow spheres) with a small fraction of atoms subsequently hit. In comparison, collision trees observed under 5 keV bombardment exhibit, on average, much more branching.[9] In contrast with heavy metal targets, one of the common characteristics of these four trees is that the trajectory of the argon atom (yellow sphere) is essentially not deflected by the numerous collisions with carbon and hydrogen atoms, which is an effect of the mass ratio between the projectile and the target atoms. As a consequence, there is no backscattering due to the organic material and the reflection of energy toward the surface, if any, is not operated via the primary particle. The collision cascade keeps the memory of the projectile trajectory in that most of the subcascades are downward directed. In some cases, the atomic collision cascade is even unable to provide the upward momentum required for fragment ejection. For this reason, we can already state that the efficiency of 500 eV Ar atom bombardment for organic material sputtering is relatively low. The lateral orientation observed for several recoil atom tracks and the ejection of atoms through the sides of the sample suggests that lateral motion is an important factor. In fact, for a molecule with this shape, we observe more lateral ejection of fragments than "true" sputtering, i.e., emission toward the vacuum.

In addition to common features, the trajectories related to Figure 4 also exhibit specifics. For instance, branching can occur either at the top (tree A) or at the bottom of the PS sample (tree C). A quick partitioning of the energy at the top of the sample (A) may lead to the efficient emission of small polyatomic fragments, as seen in section 3.1, while branching at the bottom of the sample (C) induces lateral ejection, disintegration of the sample, and, sometimes, large backbone segment ejection (see section 3.4.3, Table 2). In comparison, tree B shows very few atomic displacements. We describe in section 3.4.2 why these are good conditions for the emission of very large fragments. Finally, tree D indicates that efficient reflection of the energy via the cascade can occur when it reaches the silver substrate (see section 3.4.5). These specifics of the atomic collision cascades are detailed along the discussion.

The comparison between the snapshots of the simulation described in Figure 2 and tree A provides information about the emission of fragments induced by the atomic cascade. In this trajectory, the Ar atom dissipates about 220 eV in the first 15 fs, through the first series of collisions occurring in the top part of the sample, which is a quite unique situation with respect to the other cases shown in Figure 4. This important energy transfer induces multiple bond-breaking and leads to both sideways and upward ejection of fragments. In that sense, trajectory A constitutes an exception to the generally low sputtering efficiency mentioned in the previous paragraph. The sputtered C_6H_5 and C_9H_7 (Figure 2c and 3d) leave with 2.5 and 4.1 eV of kinetic energy, respectively, while the atomic and small molecular species ejected sideways carry more kinetic energy. Details concerning the ejected fragments are summarized in Table 2. The movie of the simulation shows quite clearly that the ejection of such polyatomic fragments is a byproduct of the hard collision between the primary particle and a direct neighbor of the fragment to be ejected. In other words, the primary Ar atom kicks off a carbon atom of the chain and, via this interaction, the fragment is set free (at least on one end) with only a few eV of kinetic energy. This mechanism is quite similar to that already reported for small polystyrene tetramers adsorbed on silver.[8]

TABLE 2: Characteristics of the Sputtered Fragments for a Subset of Trajectories (A−D) Described in the Text

fragment	mass (Da)	normal velocity (m/s)	kinetic energy (eV)	time of emission (fs)
trajectory A				
C_5H_4	60[a]/52	643	1.5	1863
C_6H_5	87[a]/77	777	2.5	2055
C_9H_7	129[a]/115	776	4.1	2420
$C_{68}H_{69}$	1024[a]/885	426	2.3	5514
trajectory B				
$C_{362}H_{359}$	5428[a]/4710	295	3.7	11557
trajectory C				
C_6H_6	90[a]/78	940	0.9	2164
$C_{106}H_{106}$	1592[a]/1380	138	2.8	4430
trajectory D				
$C_{12}H_{10}$	174[a]/154	722	1.4	5743
$C_{239}H_{240}$	3593[a]/3113	682	8.9	5562

[a] Mass of the tritiated homologue used in the simulation.

The detailed analysis of trajectory A shows that the major role of the Ar projectile regarding fragment emission is to segment the molecular backbone so that nascent secondary species are set free from the polymer coil. Another example of bond breaking, leading ultimately to the emission of a 5.4 kDa chain segment, is depicted in Figure 5. This trajectory corresponds to tree B in Figure 4. Frame 5a shows the situation after 40 fs, when the impinging Ar atom (red) is halfway through the PS sample. The red arrow indicates the aiming point of the projectile in the beginning of the simulation. Between 80 and 100 fs, the projectile breaks the C−C bond indicated by a white arrow on Figure 1c. Between 100 fs and the final snapshot at 6 ps (Figure 5c), the top part of the molecule slowly moves and rotates toward the vacuum and it is eventually ejected. This slow evolution of the excited PS sample after 100 fs is not part of the atomic cascade anymore and, therefore, it will be the object of the next section.

It would be useful to have a simple and reliable criterion to determine the transition time by which the atomic collision cascade becomes less important and molecular processes start to dominate. One possible way is to relate atomic cascade events to a given range of energy per atom. The time-evolution of the average energy per moving atom, which somehow characterizes the distribution of the primary particle energy among the atoms of the organic medium, should then indicate the transition between atomic and molecular mechanisms. In our system, it is reasonable to assume that, below a certain energy threshold corresponding roughly to the covalent binding energies in the molecule, the processes do not belong to the atomic cascade anymore because the energies become too low to displace atoms by bond breaking. Figure 6 shows the evolution of the *average* kinetic energy per moving particle as a function of time for the four trajectories used as examples in this article (A−D). For

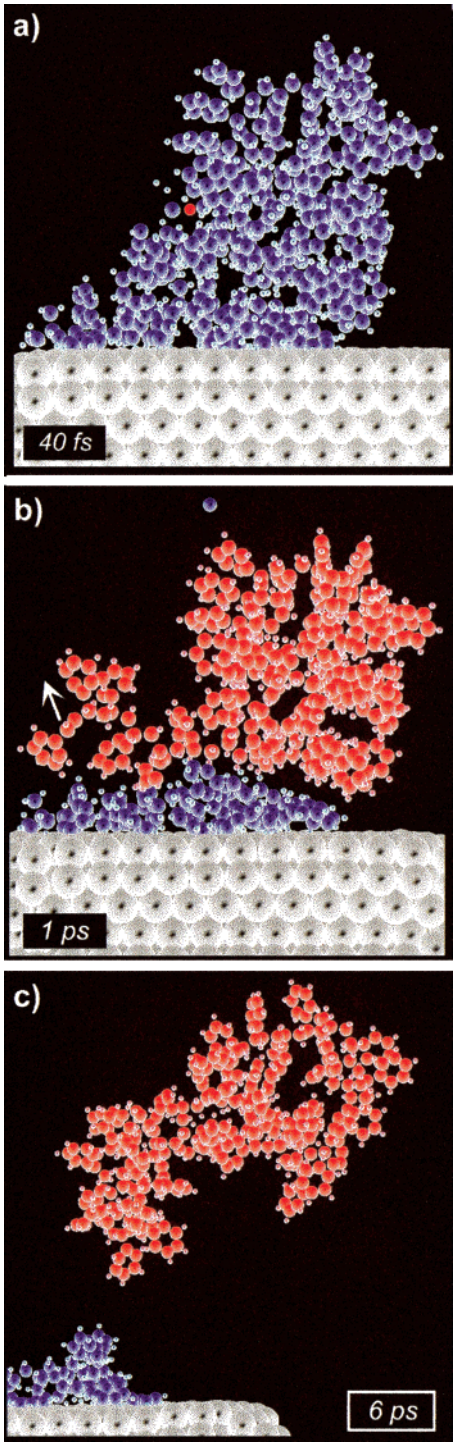

Figure 5. Time evolution of trajectory B: (a) 40 fs; (b) 1000 fs; (c) 6000 fs. The departing fragment is red.

one of the trajectories, the maximum kinetic energy possessed by any atom is represented by vertical bars. Assuming that the threshold for individual atomic motion is of the order of the bond strength in the molecule, e.g. ~5 eV, we estimate the time to be 100−300 fs. During this time period, the collision cascade is transforming from a regime dominated by atomic-like collisions into one that is controlled by molecular motions.

3.4.2. Molecular Motion and Vibrations. The movies of the trajectories and the kinetic energy curves of Figure 6 indicate that molecular processes dominate after 300 fs. Trajectory B constitutes a good basis to explore such processes. Between the bond scission at ~100 fs, already described in section 3.4.1, and the state of the sample after 1 ps (Figure 5b), very little

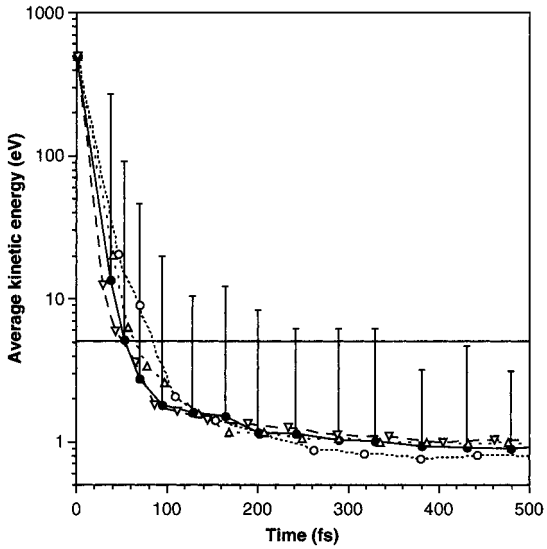

Figure 6. Time evolution of the average kinetic energy (respectively: maximum kinetic energy) of the moving atoms during the development of the collision cascade for trajectories A−D (respectively: A). See text for details.

change occurs, other than the slow rotation of the energized chain end generated by the bond breaking. During the next picoseconds, the large chain segment drifts slowly toward the vacuum without any more bond scission. The slow upward motion is accompanied by a marked change of the fragment shape. This large fragment corresponds to the formula $C_{362}H_{359}$, and its mass, considering that we used tritium instead of hydrogen in the simulation, is 5428 Da (Table 2). The emission of large-chain segments is commonly observed in other trajectories and the measured kinetic energies are, in general, comparable. Nevertheless, the genesis of such fragment ejection is unclear. Indeed, the collision that causes the bond breaking at 100 fs is not the driving force of the ejection because the internal energy of the fragment is ~120 eV, which is more than 1 order of magnitude greater than the energy transferred in that particular collision (6 eV).

To visualize the energy distribution in the cascade, we use snapshots of trajectory B in which the size and color of the atoms mirror their kinetic energy and orientation. In Figure 7, the blue-to-cyan balls are downward moving atoms, while the red-to-yellow balls are upward moving atoms. The largest ball diameter corresponds to atoms with 5 eV or more of kinetic energy. Small black dots indicate atoms with less than 0.1 eV of kinetic energy. The viewpoint is the same as Figure 5. The primary particle starts to interact strongly with the organic medium between 25 and 35 fs. After 35 fs, it has already lost 370 eV via high-energy collisions with several atoms of the sample. Figure 7a shows that after 46 fs, the momentum is mostly downward directed (blue spheres), although some atoms are ejected laterally. At that time, many of the moving atoms have more than 5 eV of kinetic energy. After the passage of fast moving recoil atoms, the bottom part of the PS sample remains excited (Figure 7b). A group of about 35 atoms still have a kinetic energy comprised between 0.5 and 3 eV. The energy of each of these atoms is too small to break bonds, but together they represent an energy excess of several tens of eV. At that time, the backbone bond scission triggering the large fragment formation has already occurred. The excited region is even more obvious after 261 fs, when all the fast atoms have left the sample (Figure 7c). The energy is localized at the bottom of the departing fragment. More than the energy transferred in

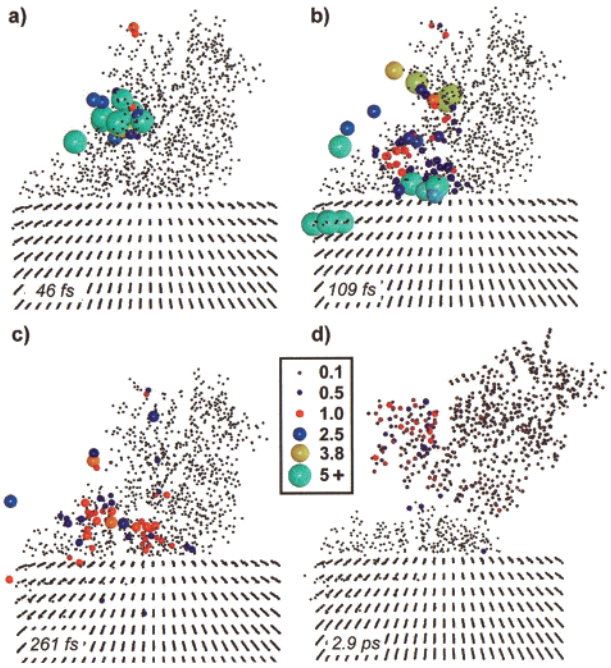

Figure 7. Picture of the kinetic energy of the atoms at different times in the development of trajectory B. Atoms moving upward are depicted by red to yellow spheres and atoms moving downward by blue to turquoise spheres. The radius of the spheres is directly proportional to the energy of the atoms up to 5 eV (see the scale in the inset). The largest radius corresponds to atoms with 5 eV or more energy: (a) 46 fs; (b) 109 fs; (c) 261 fs; (d) 2900 fs.

the bond scission described above, the energy stored in the bonds of the nascent fragment is the actual driving force of the ejection process. The last vignette (d) of Figure 7 shows that, after 2.9 ps, the internal excitation distributes over the entire fragment, which is nearly ejected.

This analysis allows us to identify the atomic collision cascade as the trigger for fragmentation and energy distribution in the organic sample, and subsequent collective motions at the molecular scale as the medium by which fragments are transferred from the surface to the vacuum. The physical link between the atomic cascade stage and the molecular motion stage, and the exact nature of the collective interaction involved, however, remains elusive. In their recent paper concerning the bombardment of crystalline benzene, the results of Krantzman et al.[13] suggest that the initial atomic cascade becomes a molecular cascade after the first few hundred femtoseconds, a time at which entire benzene molecules and fragments seem to play the role of recoil particles in the cascade. In comparison with solid benzene, our system is different in that the entire organic material is interconnected via covalent C−C bonds. Even though they are very similar to benzene molecules from the chemical viewpoint, the phenyl building blocks of our polystyrene are all strongly attached to the flexible backbone of the molecule. Therefore, the physics underlying polyatomic species emission might be different in our system.

In addition to a molecular cascade where, as defined above, small quasi-molecular entities transfer their energy via collisions with their neighbors, another extreme case of interaction would be a purely vibrational excitation of the molecular bonds, eventually leading to fragment ejection through action/reaction between the excited entity and the surrounding medium. In contrast with the concept of molecular cascade, a purely vibrational excitation is characterized by the collective but dissimilar motion of several atoms. In turn, the instant velocity vectors of moving neighbor atoms should not have the same

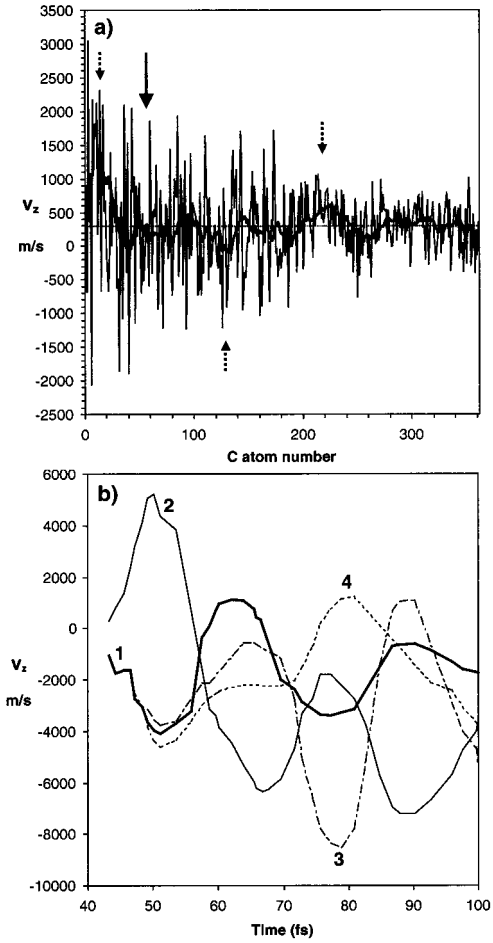

Figure 8. Normal (z) component of the velocity for C atoms ejected in trajectory B. (a) Instantaneous *z* velocity spectrum of the C atoms belonging to the sputtered $C_{362}H_{359}$ fragment at time $t = 12.5$ ps. The black arrow indicates the position of the C atoms considered in frame b. (b) Time-evolution of the *z* velocities for four neighbor C atoms in the early times of the trajectory.

orientation and amplitude. Also, as a function of time, the variation of these velocity vectors should be out-of-phase. This definition suggests that the study of the atom velocities in the sample constitutes an adequate means to reveal the physical mechanism of the molecular stage of organic sputtering.

Figure 8a shows the vertical (*z*) velocity spectrum of the C atoms belonging to the large $C_{362}H_{359}$ fragment sputtered in trajectory B, about 12.5 ps after the beginning of the interaction. The deliberate choice of studying the velocities of ejected fragments, easy to perform on a systematic basis because of the actual structure of the regular output files provided by the code, relies on the reasonable assumption that ejected fragments keep the memory of the mechanism inducing their emission. In Figure 8a, the *z* velocities are plotted as a function of the index number of the C atoms in the sample. As a result of the indexing procedure, C atoms with consecutive numbers *are always* neighbors in the molecule. Index numbers also mirror the initial position of the atoms in the sample, increasing numbers corresponding roughly to an increasing height in the quasi-helical structure shown in Figure 1b,c. For these reasons, the velocity spectrum of Figure 8a provides us with information concerning the amplitude of the velocities *and* with a qualitative estimate of the velocity correlation among neighbor atoms in the PS sample. First, the velocity spectrum is centered around the fragment center-of-mass velocity, that is 295 m/s (dashed line in Figure 8a). Second, it is obvious that the C atom

velocities are often much larger than the center-of-mass velocity, especially in the lower-half of the fragment, where they can be almost an order of magnitude higher. Third, and most importantly, the spectrum is characterized by a very pronounced variation of the *z* velocities between neighbors, most of the paired neighbors moving in opposite directions with respect to the *z* axis. Fourth, the decreasing amplitude of the oscillations with increasing index number indicates that the delocalization of the internal energy is still incomplete after 12.5 ps, the bottom part of the fragment remaining more excited than the top part. Finally, the moving average of the velocities (thick line) points to the existence of domains in the molecule whose local centers-of-mass are slower or faster than the overall center-of-mass velocity (dashed arrows). However, the second and third comments also apply to these restricted domains.

The second and third observations suggest that the nature of the collective motion giving rise to large fragment ejection relates more to the above concept of vibrational excitation as opposed to that of molecular cascade. Nevertheless, the final observation supports the idea that there is a weak correlation between atomic motions in several parts of the molecule. For instance, this is true for the rotating chain end of the fragment (Figure 5). Similar observations and conclusions are generally true for large fragments sputtered in the simulation.

For trajectory B, we also analyzed the initial state of the departing fragment. Figure 8b shows the time evolution of the *z* velocity vectors of four C atoms that are neighbors in the nascent fragment, from the time they are set in motion (40 fs) until a time of 100 fs. Geometrically, atoms 1−4 are aligned in a row in the sample, so that atom 2 is surrounded by atoms 1 and 3 and atom 3 by atoms 2 and 4. They all start moving at an approximate time of 42 fs, as a result of the passage of the Ar atom in their vicinity (see the description of Figure 7). Atoms 1, 3, and 4 first move downward while atom 2 moves upward. Over the time span encompassed in Figure 8b, these atom velocities oscillate between positive and negative values, with the velocity of direct neighbors almost being of opposite phase. Therefore, we can state that the vibrational nature of the collective motion is established in the first few femtoseconds following its induction by the atomic collision cascade. As was assumed, the final state of the ejected fragment mirrors the early stage of collective motion in the bombarded molecule.

The exact shape of the collision tree (Figure 4) and the size of the ejected fragments vary for different trajectories (see Figures 2 and 5 and Table 2). Regardless of the specifics, the bombardment generally induces a localized vibrational excitation of the molecular bonds after the atomic cascade phase of the atom−solid interaction. This excitation is long-lived, because the energy excess per bond is generally too low to be released via bond breaking. With time, the excitation energy tends to delocalize over the whole PS sample or fragment, provided that it constitutes an interconnected network of covalent bonds. The energy stored in the sample or fragment leads oftentimes to its swelling or even to its ejection. In some instances, it can also induce unimolecular decomposition reactions, as described in the next section.

3.4.3. Unimolecular Decomposition Reactions. In SIMS of organic materials, unimolecular decomposition of ejected fragments is a well-established phenomenon. Metastable decay of excited secondary ions *in the vacuum* is experimentally observed in time-of-flight spectrometers including either ion mirrors or electrostatic analyzers.[28−31] On the other hand, the decomposition of excited organic molecules *on the surface* cannot be assessed by experimental means. In this domain, MD simulations provide useful predictions and insights.

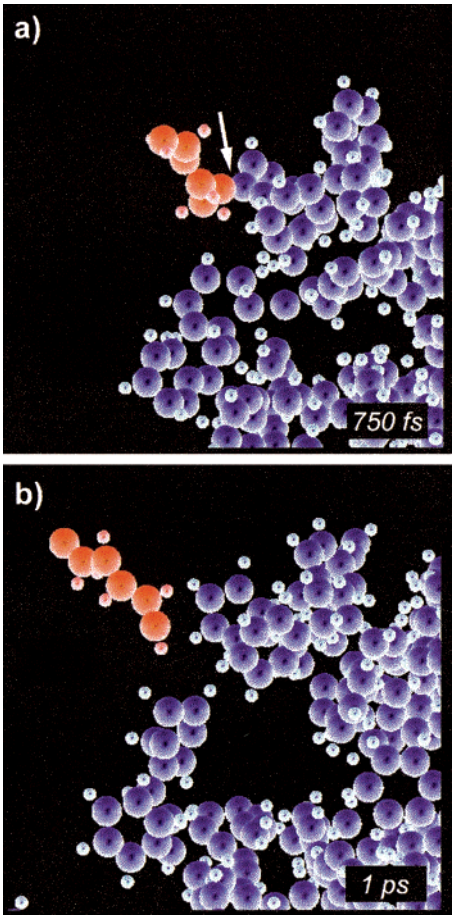

Figure 9. Close-up views of the time evolution of trajectory C. (a) 750 fs; the white arrow points to the C−C bond that will be severed by vibrations. (b) 1000 fs. The nascent C_6H_6 is red.

Figure 9 describes a trajectory in which a linear C_6H_6 fragment is formed via unimolecular dissociation of the excited PS sample (trajectory C) before the larger fragment ejects (Table 2). The collision tree of trajectory C is depicted in Figure 4. Figure 9a presents a close-up view of the sample top left part at 750 fs. This region has been damaged by the projectile and a linear chain segment is dangling into the vacuum. The white arrow in Figure 9a points to the C−C bond that is going to break between 750 fs and 1 ps. After 1 ps, the linear C_6H_6 fragment is ejected but unstable,[8] with 14.2 eV of internal energy (Figure 9b). To our knowledge, it is the first time that the formation of secondary species via unimolecular dissociation of excited molecules *before* ejection is reported. Such a process could not be identified in our previous study of small polystyrene tetramers, where the ejection of fragments was mostly due to atomic collision mechanisms.[8] This result allows us to predict that vibration-induced fragmentation, caused by an energy excess in the backbone bonds, should be significant for large organic molecules and polymers bombarded by keV ions.

3.4.4. Recombination and Rearrangement Reactions. Other reaction pathways might coexist in addition to vibration-induced decomposition of the organic sample on the surface and metastable decay of ejected fragments. Of crucial importance for SIMS analysis are the possible recombination and rearrangement reactions supposed to occur through the emission process.[32−34] In particular, extensive recombination reactions would be a major problem since such reactions scramble the structural information provided by the mass spectrum. Below

TABLE 3: Fraction of the Ejected Fragments Formed via Recombination Reactions

C_2	C_2H	C_2H_2	C_5H	C_5H_3	C_4H_4	C_5H_5	C_6H_5	C_6H_6	C_7H_6	100−200 Da	> 500 Da
5/10 (50%)	12/48 (25%)	5/95 (5%)	2/10	none	none	none	none	none	none	1/12	none

SCHEME 1: Recombination Reaction Leading to the Formation of a C_9H_7 Fragment

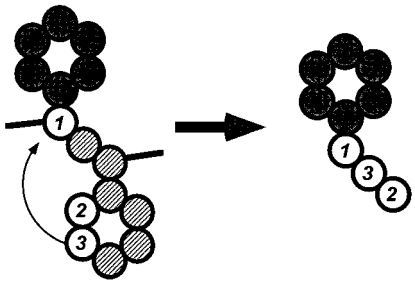

we delineate these issues using the detailed information on ejected fragments present in the simulation results.

To perform a systematic study of the recombination and rearrangement reactions occurring in the course of the emission process, the lists of neighbors of each C atom belonging to the sputtered fragments are compared to their original neighbors in the relaxed PS sample, prior to emission. Hydrogen capture or hydrogen exchange reactions are not discussed here for two reasons. First, they have already been investigated in previous papers for the cases of adsorbed alkyl chains[35] and styrene tetramers[8] and, second, their consequences for the interpretation of experimental mass spectra are much less dramatic. Changes in the C atom neighbor lists can either show the association of atoms or fragments that were initially apart in the sample (recombination) or the exchange of atomic positions in the considered molecular segments (rearrangement), possibly leading to a different structure.

The information concerning recombination reactions is summarized in Table 3 for the results using the AIREBO interaction potential. When it is appropriate, the fraction assigned to each fragment shows the number of those species formed via a recombination process divided by their total number in the simulation set. There are also fragments for which no recombination reactions are observed ("none" in Table 3). The results indicate that recombination reactions are significant for very small fragments ($C_2-C_2H_2$), and more so for hydrogen-deficient fragments. Beyond 40 Da, they constitute rare events. In the range 100−200 Da, only one fragment out of twelve arises from a recombination process involving two smaller fragments. In that particular case, the final product is a C_9H_7, formed by the association of a C_2H_2 and a C_7H_5. The initial and final situations are depicted in Scheme 1. The hatched spheres correspond to C atoms that do not belong to the final fragment. Note that the formation of this C_9H_7 fragment requires four C−C bond scissions, the elimination of a H atom and the creation of a new C−C bond. The dynamics of the trajectory shows that the recombination reaction occurs at a time when the two fragments are still within the interaction range of the remaining system.

Although rearrangement reactions are not predominant, they also occur during the cascade development, the sputtering process or even after emission. In this context, a rearrangement reaction is defined by a change of the neighbor lists of C atoms that were already interconnected in the sample prior to emission, but with a different order. An example of rearrangement reaction concomitant with emission is described in Scheme 2. The initial chain segment comprises four styrene repeat units bound to the rest of the molecule at both ends. In the course of the sputtering process, one carbon atom and one phenyl ring are eliminated, and the two C−C bonds linking the segment to the sample are severed. Furthermore, in parallel with the bond scissions, atom 1 and the atom pair 2−3 swap positions in the chain, whereas the phenyl-containing atom 5 disconnects from atom 4 and binds with atom 6. Such a gross structural change is possible only because the internal energy of the chain segment is high. Due to its internal excitation, the fragment described in Scheme 2 has a very low probability to survive beyond a nanosecond without undergoing further fragmentation reaction.

SCHEME 2: Rearrangement Reaction in a $C_{24}H_{18}$ Fragment

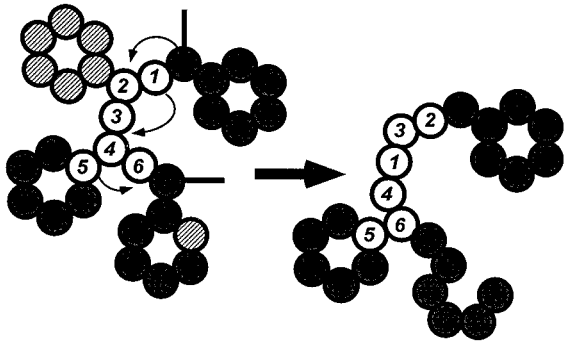

In conclusion, recombination and rearrangement reactions are observed in the simulation. Nevertheless, for the SIMS user, the fact that very few fragments with a mass of more than 40 Da arise from such reactions is reassuring. In this respect, MD simulations support the concept of structural specificity of the SIMS analysis.

3.4.5. Substrate Effect. It has been mentioned that the collision cascade caused by the Ar projectile could in some instances be partially reflected by the silver substrate. This mechanism is illustrated by the collision tree of trajectory D (Figure 4). In this trajectory, the primary particle plunges through the top part of the polystyrene sample without strong interaction with the surrounding medium and dissipates most of its energy a few Angstroms above the metal surface. Several of the recoil carbon atoms are backscattered by the silver plane, and a few silver atoms are displaced in the process. Figure 10 shows three snapshots of trajectory D. The influence of the momentum reflection at the PS−metal interface is not yet obvious at 750 fs. Nevertheless, at this time, the energy is already stored in the right part of the PS sample which starts moving upward. After 2 ps, the influence of the reflected energy is evident and the organic material is expanding toward the vacuum. As was observed for trajectory B, the early collision-induced bond scissions lead to the sputtering of the top part of the sample after a few picoseconds (Figure 10c).

Because of the relatively small number of calculated trajectories, it is difficult to extract quantitative information on the influence of the PS−silver interface using MD simulations. To obtain complementary statistics concerning the effect of the interface, TRIM calculations[36,37] have been performed using a sample constituted of a 25 Å overlayer of hydrocarbon material mimicking polystyrene on top of a thicker layer of silver. The pseudo-organic layer, provided by the compound library of the

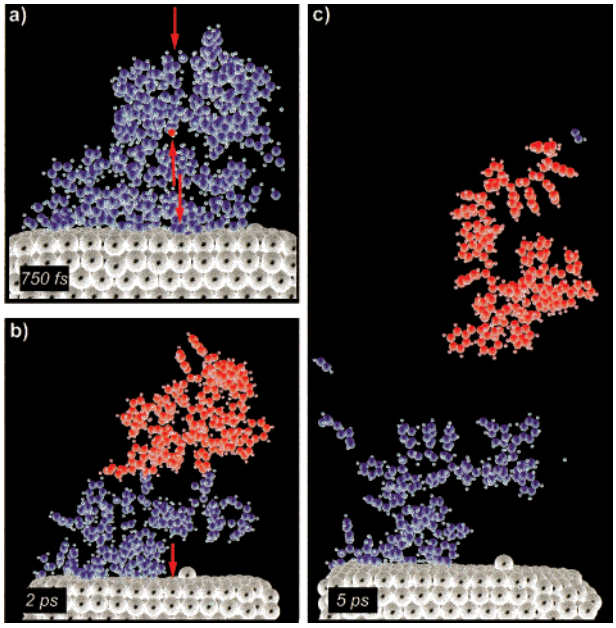

Figure 10. Time evolution of trajectory D. (a) 750 fs; the red arrows indicate the position of the impact and the pathway of the Ar atom through the polystyrene coil. (b) 2000 fs; (c) 5000 fs. The departing $C_{239}H_{240}$ chain segment is red.

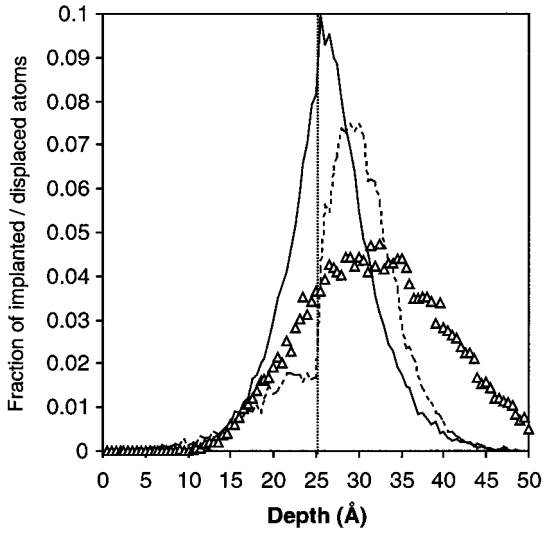

Figure 11. TRIM simulation of the depth distribution of implanted Ar projectiles in a bulk polystyrene sample (triangles) and in a 25 Å polystyrene overlayer on silver (full line). The dashed line shows the distribution of displaced silver atoms at the end of the trajectories for the thin PS overlayer.

software, has the stoichiometric C:H ratio and the density (1.06 g/cm^3) of PS. TRIM assumes different displacement energies for the C, H, and Ag atoms, which mirror the bond strengths in the solid. Of course, due to the binary collision approximation, cooperative and vibrational effects are completely neglected. Therefore, TRIM gives, at best, a frozen image of the sample after the atomic cascade stage of the interaction. This partial view is reasonable if the atomic and collective motion stages of the interaction are decoupled. Out of prudence, we limit our analysis of the TRIM results to the depth distribution of projectiles and recoil atoms in the solid. The collision trees (Figure 4) and the average energy vs time curves (Figure 6) show that these distributions are established in the first few hundred femtoseconds of the interaction, mostly before the onset of collective vibrational motions.

The distributions of ranges of the primary Ar atoms in the solid are shown in Figure 11 for a bulk PS sample (open triangles) and for a thin PS overlayer on Ag (full line). Due to the larger stopping power of the Ag substrate, the range distribution corresponding to the thin-layered PS sample is squeezed around the polymer/silver interface, in comparison with the much broader distribution observed for the bulk PS sample. The average range is consequently reduced from 31 Å (bulk PS) to 26 Å (thin PS). Therefore, in agreement with the MD results, TRIM confirms that the effect of the substrate is significant for the chosen conditions of primary particle energy and organic layer thickness. The final distribution of the silver recoil atoms provided by TRIM (dashed line) is also indicative of the momentum reflection at the interface. Indeed, a significant fraction of the displaced Ag atoms is implanted in the upper PS layer at the end of the trajectories, mainly in the first 15 Å above the interface.

3.5. Experimental Evidence. The comparison of MD simulation results with experimental data is an important issue. In previous work, we validated the MD model by comparing the calculated mass spectra and kinetic (KED) and angular distributions of ejected species to their experimental counterpart.[4,7,8] In the case of regular SIMS experiments, the comparison is somewhat indirect because the sputtered species have to become ions through the emission process in order to be measured as yield. For this reason, the effects of the sputtering and ionization processes cannot be easily distinguished. For PS oligomer overlayers on silver, the SIMS spectra indicate that entire molecules and large molecular fragments need to capture an Ag adduct to become ionized.[38] Because the intensity of organometallic aggregates is very low in the MD simulation, we cannot use these species for a comparison with experimental results, as discussed in ref 8. Alternatively, it is possible to compare the yields and distributions observed for single molecules and fragments in the simulation with their Ag-cationized homologues in the experiment. In a previous paper, the calculated KED of short polystyrene oligomers sputtered from a silver surface under 500 eV Ar bombardment has been compared to the experimentally measured KED of Ag-cationized homologues emitted under 15 keV Ga^+ bombardment.[8] Despite the different energies, the KEDs were surprisingly similar. A more recent MD investigation with 5 keV Ar atoms shows that the influence of the primary particle energy on the KEDs is not marked, except for the high-energy tail of the distribution, which is slightly more pronounced at 5 keV because of the advent of a new emission mechanism involving large-scale collective events in the silver substrate.[9] Because of this low sensitivity to the primary particle properties and to the exact nature of the sputtered species, we believe it is reasonable as well to compare our new simulation results with 15 keV Ga^+ ion-induced desorption of large PS fragments.

The ToF−SIMS spectrum of deuterated polystyrene PS oligomers cast on silver is shown in Figure 12. The number average molecular weight (M_n) of the PS oligomers is ~5300 Da, that is, the maximum of the distribution should correspond to PS oligomers with ~47 repeat units, which is not too far from the PS sample used in the model. Figure 12a shows the high-mass range of the SIMS spectrum, between 700 and 3500 Da, where large fragments are expected to appear. In this mass range, two significant series of peaks can be noticed. The first series looks like an intense background noise that decreases exponentially as a function of mass. In fact, this noise is mainly constituted by Ag-cationized PS fragments, as is shown hereafter. The second series of peaks, reflecting the entire oligomer distribution, corresponds to silver-molecule aggregates

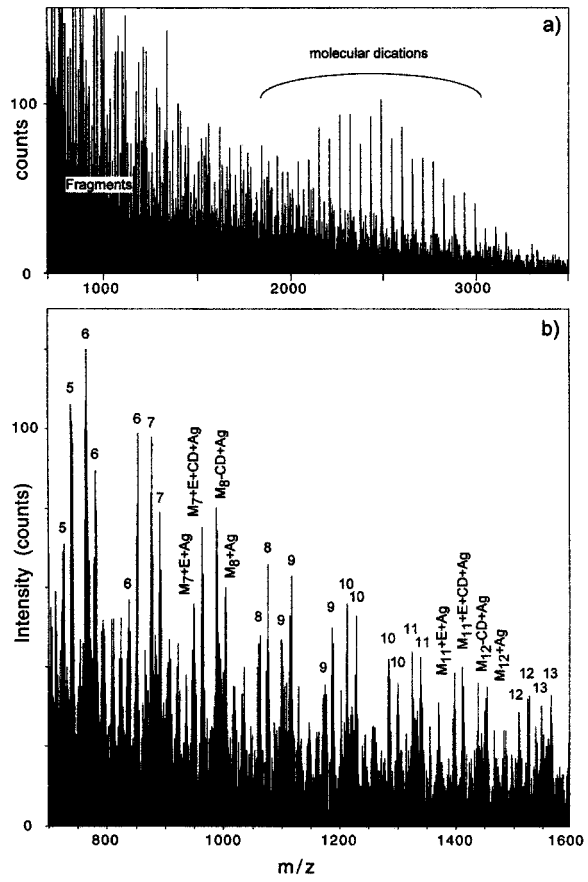

Figure 12. Experimental mass spectrum of *sec*-butyl terminated deuterated PS oligomers (M_n = 5300) adsorbed on a polycrystalline Ag foil. Top frame: high mass region of the spectrum. Bottom frame: zoom on the fragmentation part of the high mass region. The formulas refer to the identification of the silver-cationized fragments (see text for details).

bearing two positive charges. The double-cationization process is indicated by the frequency of the peaks, occurring every 56 Da instead of 112 Da (deuterated PS), and by the maximum of the distribution, around 2.6 kDa. These are about half the expected values, because dications acquire twice the kinetic energy of single cations in the electric field. Therefore, their time-of-flight is shorter than that of monocations by a factor $\sqrt{2}$ and their calculated mass is half the mass of monocations. This observation and its analytical consequences will be discussed at length in a future experimental paper.

In the discussion, we focus on the large fragment series that can be compared to the simulation results. Nevertheless, it is important to mention why entire molecules are sputtered in the experiment and not in the simulation. The reason entire molecules are not ejected in the MD model is probably twofold. First, we chose to direct all the aiming points toward the molecule itself, and it has been shown in previous studies that entire molecules are emitted almost exclusively when the projectile aims at the surrounding silver surface, via a collision cascade process in the metal surface.[8] Second, the projectile energy is much lower in the simulation than in the experiment, and we showed that the emission of several kDa molecules requires the development of large-scale collective motions in the substrate, a situation that is not observed with 500 eV impinging particles.[9]

What appears at first sight as background noise in Figure 12a is actually a well-structured sequence of peaks. An expanded view of the mass range 700−1600 Da is displayed in Figure 12b. This region encompasses eight occurrences of a similar pattern constituted by four main peak series. As indicated by the labels in two cases, the formulas corresponding to the different peak series are $(M_x+Ag)^+$, $(M_x-CD+Ag)^+$, $(M_x+E+Ag)^+$ and $(M_x+E+CD+Ag)^+$, where M is the deuterated styrene repeat unit and E is the *sec*-butyl endgroup. The repetition period of the pattern is given by the mass of the deuterated styrene repeat unit, M = 112 Da. The nature of the detected fragments indicates that the macrochains can break almost statistically at any backbone bond, ejecting chain segments including one or the other chain end with an equal probability. In parallel, the emission probability decreases regularly with increasing fragment size. The structure of the observed fragments, e.g. $(M_x+Ag)^+$, $(M_x-CD+Ag)^+$, agrees very well with the MD simulation results (Figure 3c), if one omits the Ag adduct. The fact that the series of fragments including the butyl endgroup, $(M_x+E+Ag)^+$ and $(M_x+E+CD+Ag)^+$, are not sputtered in the simulation is most probably due to the chosen initial conditions. Indeed, the arrangement of both PS oligomers in the model is such that the butyl endgroups are located on the bottom of the organic samples, at the interface with the Ag substrate. Obviously, this configuration makes large fragments including the butyl endgroup more difficult to eject. From the comparison, we can deduce that large fragments of PS oligomers and similar molecules will be emitted more likely if they are located on top of the sample.[26] Although the process is more complex here, the same effect has also been noticed for much smaller upright chains of alkyl[39] and thiol molecules.[7]

In summary, the comparison between experiment and simulation indicates that the fragmentation pattern of PS oligomers is well described by the model, even though the molecular arrangement chosen in the simulation represents only one of the many possible configurations sampled in the experiment. Remarkably, the nature of the sputtered fragments is sensitive to the molecular orientation.

4. Conclusion

Particle bombardment induces a variety of physical and chemical processes in a large organic sample such as the 61 repeat unit PS oligomer we chose for this study. A part of these mechanisms are a direct transposition of the processes induced in smaller organic molecules, e.g., the atomic collision-induced emission of atomic and small polyatomic fragments. Other processes are observed for the first time, such as the development of the atomic collision cascade inside the polymer coil. A second phenomenon is the transition from an atomic cascade regime, where atoms collide much like billiard balls, to a molecular motion regime, where the energy is stored in the vibration and rotation modes of the molecule and the motions become collective. Our analysis points to a true vibrational excitation, where the atomic motions are collective but the velocity vectors are broadly distributed, rather than a molecular cascade, where groups of atoms with a correlated motion would play the role of atoms in the cascade. We identified two steps in the molecular phase of the interaction. First is the excitation of a few bonds surrounding the locus of interaction with the projectile or a recoil atom and afterward, the slow delocalization of vibrational energy over the whole molecule or fragment, which can take more than 10 ps. Typically, the internal kinetic energy per atom is close to 0.1 eV for large vibration-induced fragments. In some instances, the concentration of the available

energy in a small set of C−C bonds also leads to the decomposition of the molecule, through the delayed emission of excited fragments. Recombination reactions are also observed, but they mainly affect very small hydrogen-deficient species, and not larger fragments. The ejection of large molecular segments can also be assisted by the reflection of the projectile and recoil atom energy on the silver substrate.

More technically, the comparison of the REBO and AIREBO potentials has been performed and the sputtering results are significantly dependent on the choice of potential. In particular, the sputtering yield of polyatomic fragments is reduced by the introduction of long-range attractive forces. The arrangement of the molecule on the surface and the choice of the target area also affect the sputtering yields.

Although the mass spectrum provided by the model is truncated with respect to the real SIMS spectrum, the large fragment peaks observed in the simulation have their homologue in the experiment. In comparison, the simulation data are partial because a limited set of molecular orientations and aiming points have been investigated, while the experiment statistically samples the whole set of possible configurations. For a further comparison involving energy distributions, the projectile energy and the number of calculated trajectories should be increased by an order of magnitude in the simulation, which involves prohibitive CPU time costs with the AIREBO potential. The implementation of ionization schemes in the MD model is also desirable, but it remains very difficult to achieve and can only be seen as a long-term goal. In future works, we plan to vary the sputtering parameters, e.g., different projectile energy and incidence angle, polyatomic projectiles, and to study other hydrocarbon systems. For instance, in parallel with the development of matrix-enhanced SIMS, we plan to model the ejection of PS oligomers embedded in a low molecular weight organic matrix.

Acknowledgment. The authors thank Kristin Krantzman (College of Charleston, USA) for helpful discussion and advice as well as Karsten Reihs (Bayer Ag, Leverkusen, Germany) who kindly provided the deuterated PS sample. Steve Stuart provided the source code for the AIREBO potential and has answered numerous questions about it. The financial support of the National Science Foundation through the Chemistry Division, the CRIF program, and the MRI program is gratefully acknowledged by A.D. and B.J.G. Additional computational resources were provided in part by the IBM Selected University Resource Program and the Center for Academic Computing of Penn State University. We are also indebted to the Center for Academic Computing staff for helping us use the IBM SP computer and for the development of a new graphics software for animation and presentation. A.D. also acknowledges the Belgian *Fonds National pour la Recherche Scientifique* for financial support. The ToF-SIMS equipment was acquired with the support of the *Région Wallonne* and *FRFC-Loterie Nationale* of Belgium.

References and Notes

(1) *Secondary Ion Mass Spectrometry, SIMS XII Proceedings*; Benninghoven, A., Bertrand, P., Migeon, H.-N., Werner, H., Eds; Elsevier: Amsterdam, 2000.

(2) Delcorte, A. Fundamental Aspects of Organic SIMS in *ToF−SIMS: Surface Analysis by Mass Spectrometry*; Vickerman, J. C., Briggs, D., Eds.; SurfaceSpectra/IM Publications: Manchester, in press.

(3) Garrison, B. J.; Delcorte, A.; Krantzman, K. D. *Acc. Chem. Res.* **2000**, *33*, 69.

(4) Chatterjee, R.; Postawa, Z.; Winograd, N.; Garrison, B. J. *J. Phys. Chem. B* **1999**, 103, 151.

(5) Townes, J. A.; White, A. K.; Wiggins, E. N.; Krantzman, K. D.; Garrison, B. J.; Winograd, N. *J. Phys. Chem. B* **1999**, *103*, 4587.

(6) Taylor, R. S.; Garrison, B. J. *Langmuir* **1995**, *11*, 1220.

(7) Liu, K. S. S.; Yong, C. W.; Garrison, B. J.; Vickerman, J. C. *J. Phys. Chem. B* **1999**, *103*, 3195.

(8) Delcorte, A.; Vanden Eynde, X.; Bertrand, P.; Vickerman, J. C.; Garrison, B. J. *J. Phys. Chem. B* **2000**, *104*, 2673.

(9) Delcorte, A.; Garrison, B. J. *J. Phys. Chem. B* **2000**, *104*, 6785.

(10) Beardmore, K.; Smith, R. *Nucl. Instrum. Methods B* **1995**, *102*, 223.

(11) Brenner, D. W. *Phys. Rev. B* **1990**, *42*, 9458.

(12) Stuart, S. J.; Tutein, A. B.; Harrison, J. A. *J. Chem. Phys.* **2000**, *112*, 6472.

(13) Krantzman, K. D.; Postawa, Z.; Garrison, B. J.; Winograd, N.; Stuart, S.; Harrison, J. A. *Nucl. Instrum. Methods B* **2001**, *180*, 159.

(14) Kerford, M.; Webb, R. P. *Nucl. Instrum. Methods B* **2001**, *180*, 44.

(15) Complementary information concerning these simulations can be found at the following Internet address: http://www.ee.surrey.ac.uk/SCRIBA/simulations/

(16) Williams, P.; Sundqvist, B. U. R. *Phys. Rev. Lett.* **1987**, *58*, 1031.

(17) Harrison, D. E., Jr. *CRC Crit. Rev. Solid State Mater. Sci.* **1988**, *14*, S1.

(18) Garrison, B. J.; Winograd, N.; Harrison, D. E., Jr. *J. Chem. Phys.* **1978**, *69*, 1440.

(19) Winograd, N.; Garrison, B. J. In *Ion Spectroscopies for Surface Analysis*; Czanderna, A. W., Hercules, D. M., Eds.; Plenum Press: New York, 1991; p 45.

(20) Garrison, B. J. *J. Chem. Soc. Rev.* **1992**, *21*, 155.

(21) Bernardo, D. N.; Bhatia, R.; Garrison, B. J. *Comput. Phys. Commun.* **1994**, *80*, 259.

(22) Brenner, D. W. *Phys. Rev. B* **1990**, *42*, 9458.

(23) Brenner, D. W.; Harrison, J. A.; White, C. T.; Colton, R. J. *Thin Solid Films* **1991**, *206*, 220.

(24) Daniels, C. A. *Polymers: Structure and Properties*; Technomic Publishing: Lancaster, Pennsylvania, 1989.

(25) Schueler, B. W. *Microsc. Microanal. Microstruct.* **1992**, *3*, 119.

(26) Pacholski, M. L.; Cannon, D. M.; Ewing, A. G.; Winograd, N. *J. Am. Chem. Soc.* **1999**, *121*, 4716.

(27) Delcorte, A.; Garrison, B. J. *Nucl. Instrum. Methods B* **2001**, *180*, 37.

(28) Delcorte, A.; Bertrand, P. *Int. J. Mass Spectrom.* **1999**, *184*, 217.

(29) Schueler, B.; Beavis, R.; Ens, W.; Main, D. E.; Tang, X.; Standing, K. G. *Int. J. Mass Spectrom. Ion Processes* **1989**, *92*, 185.

(30) Feld, H.; Leute, A.; Rading, D.; Benninghoven, A.; Chiarelli, D.; Hercules, D. M. *Anal. Chem.* **1993**, *65*, 1947.

(31) Gilmore, I.; Seah, M. P. *Appl. Surf. Sci.* **1999**, *144/145*, 26.

(32) Murray, P. T.; Rabalais, J. W. *J. Am. Chem. Soc.* **1981**, *103*, 1007.

(33) Michl, J. *Int. J. Mass Spectrom. Ion Phys.* **1983**, *53*, 255.

(34) Snowdon, K. *Nucl. Instrum. Methods B* **1985**, *9*, 132.

(35) Taylor, R. S.; Garrison, B. J. *J. Am Chem. Soc.* **1994**, *116*, 4465.

(36) Biersack, J. P. in *Ion Beam Modification of Materials*; Mazzoldi, P., Arnold, G. W., Eds.; Elsevier: Amsterdam, 1987; p 648.

(37) Information concerning this program can be found at the following Internet address: http://www.research.ibm.com/ion-beams/SRIM/

(38) Delcorte, A.; Bertrand, P. *Surf. Sci.* **1998**, *412/413*, 97.

(39) Taylor, R. S.; Garrison, B. J. *Chem. Phys. Lett.* **1994**, *230*, 495.